# 2011 SNM Highlights Lecture

*From the Newsline Editor: The Highlights Lecture, presented at the closing session of each SNM Annual Meeting, was originated by and presented for more than 33 y by Henry N. Wagner, Jr., MD. Beginning in 2010, the duties of summarizing selected significant presentations at the meeting were divided among 4 distinguished nuclear and molecular medicine subject-matter experts. These same experts presented the 2011 Highlights Lecture on June 8 at the SNM Annual Meeting in San Antonio, TX. The first 2 presentations are included here, and the remaining 2 will appear in the November issue of Newsline. Peter Herscovitch, MD, cochair of the SNM Scientific Program Committee, introduced Markus Schwaiger, MD, and Christopher Rowe, MD, who spoke on cardiology and neuroradiology, respectively. Note that in the following presentation summaries, numerals in brackets represent abstract numbers from* The Journal of Nuclear Medicine *(2011;52[suppl 1]).*

## Cardiovascular

In 2011, 125 (97 clinical, 28 basic sciences) presentations on cardiovascular topics were given at this meeting, compared with 130 (80 clinical, 50 basic sciences) in 2010. The geographic distribution in 2011 was relatively unchanged from 2010, with 65 abstracts from the Americas, 33 from Europe, and 27 from Asia and the Pacific. Myocardial perfusion (MP) continued to play a strong role, and we saw a slight shift toward PET imaging and a noticeable increase in interest in hybrid imaging. At this meeting 14 abstracts were on molecular, 21 on hybrid, 9 on vascular, and 16 on SPECT/MP imaging, with 8 on cardiac resynchronization therapy/dyssynchrony, 18 on methods, and 15 classified as "other."

### Methods and Tracers

The isolated heart is one of the major tools in cardiovascular investigative science. Madar et al. from the Johns Hopkins Medical Institution (Baltimore, MD) reported on "Novel techniques for dynamic PET imaging in guinea pig isolated perfused heart, including $^{18}$F-FBnTP distribution and kinetics" [333]. By combining various tools, they were able to demonstrate with high-resolution dynamic data the ability to image the entire perfused heart and looked at various physiologic parameters, such as perfusion extraction and tracer kinetics with or without therapeutic or pharmacologic interventions. Figure 1 shows results in guinea pig hearts, and it remains to be seen whether this model can be extended to the human heart.

**Markus Schwaiger, MD**

Clinical instrumentation in SPECT was dominated by further evaluation of high-speed dedicated cardiovascular cameras. Several presentations demonstrated the possibility of either shortening acquisition times or lowering doses to patients without great loss in image quality. For example, Nkoulou et al. from University Hospital Zurich (Switzerland) reported that a "Cadmium-zinc-telluride gamma camera allows quarter-dose MPI SPECT" [445] (Fig. 2). They showed that changes on rest and stress defects were quite acceptable and emphasized the decreased radiation exposure to the patient.

Meden et al. from the University of Michigan Medical Center (Ann Arbor) reported on "Clinical comparison of 4-mm IQ-SPECT imaging with conventional parallel-hole collimated SPECT/CT" [1132]. These authors showed they could speed up acquisition by collimator and software approaches. Figure 3 shows data from James Corbett, MD, from this group, indicating again that by having a special collimator and data processing, typical SPECT acquisition time can be reduced from 18 to 4 min without

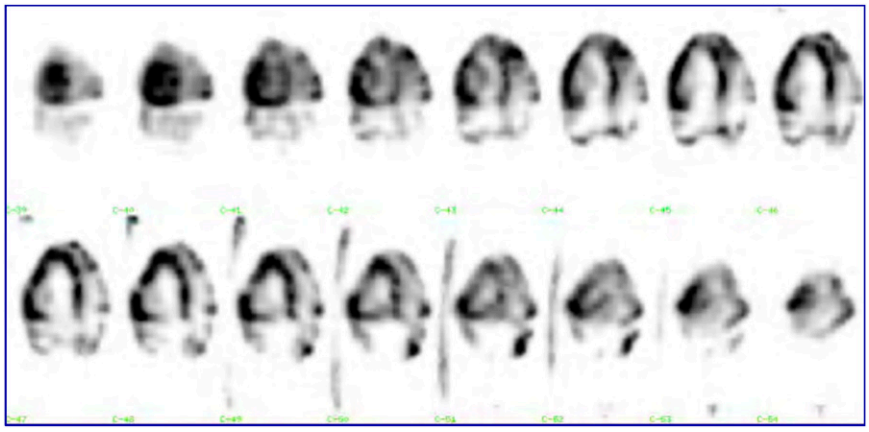

**FIGURE 1.** $^{18}$F-FBnTP distribution and kinetics in guinea pig perfused heart. Long-axis images acquired over 5–15 min postadministration (output and input lines are visible). Peak activity in input line, obtained at time of injection, dropped by 95% within 10–20 s. Peak activity in left ventricular (LV) wall, obtained at time of injection, dropped by 30%−40% within 10–20 s. LV wall activity increased to 160%−200% of baseline within 20 min.

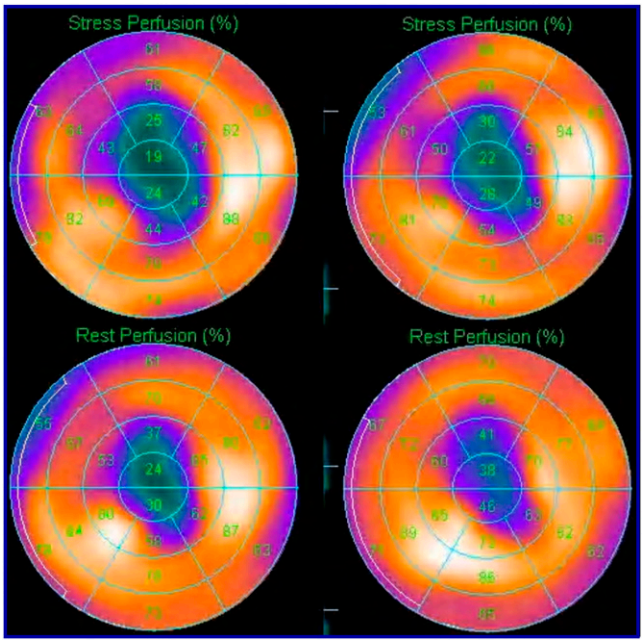


**FIGURE 2.** MPI SPECT with cadmium-zinc-telluride camera using quarter-dose $^{99m}$Tc-tetrofosmin activity. Left: quarter dose; right: standard dose.

detrimental effects on image quality or quantitative analysis of the data.

$^{82}$Rb was the most widely reported PET MP tracer at this meeting. However, much of the initial work was obtained with 2D PET instrumentation. Questions about the quality of 3D data acquisition and quantitation of regional rubidium uptake and blood flow remain unanswered. These questions were addressed by Yoshinaga et al. from the Hokkaido University Graduate School of Medicine (Sapporo, Japan) and the Ottawa Heart Institute (Canada), who reported on "Quantification of regional myocardial blood flow [MBF] using 3D $^{82}$Rb PET: comparison with 2D $^{82}$Rb data acquisition" [386]. Data showed good agreement between global left ventricular (LV) MBF at stress and flow reserve, but the polar map shows significant heterogeneity (Fig. 4). This emphasizes the need for quality control in rubidium PET studies, where the prompt $\gamma$ is produced in the rubidium decay and the 2 single protons arise from the positron decay. The technical challenge is to avoid any scatter effects that may act regionally.

However, analysis of MP measurements and calculation of global and rest flow are quite reproducible and robust, as seen in the study by Sunderland et al. from the University of Iowa (Iowa City), who reported on "Interobserver variability in $^{82}$Rb measured blood flow and coronary flow reserve [CFR] measurements" [1112]. They compared automated analysis with that of 3 observers, showing excellent agreement for absolute flow measurements.

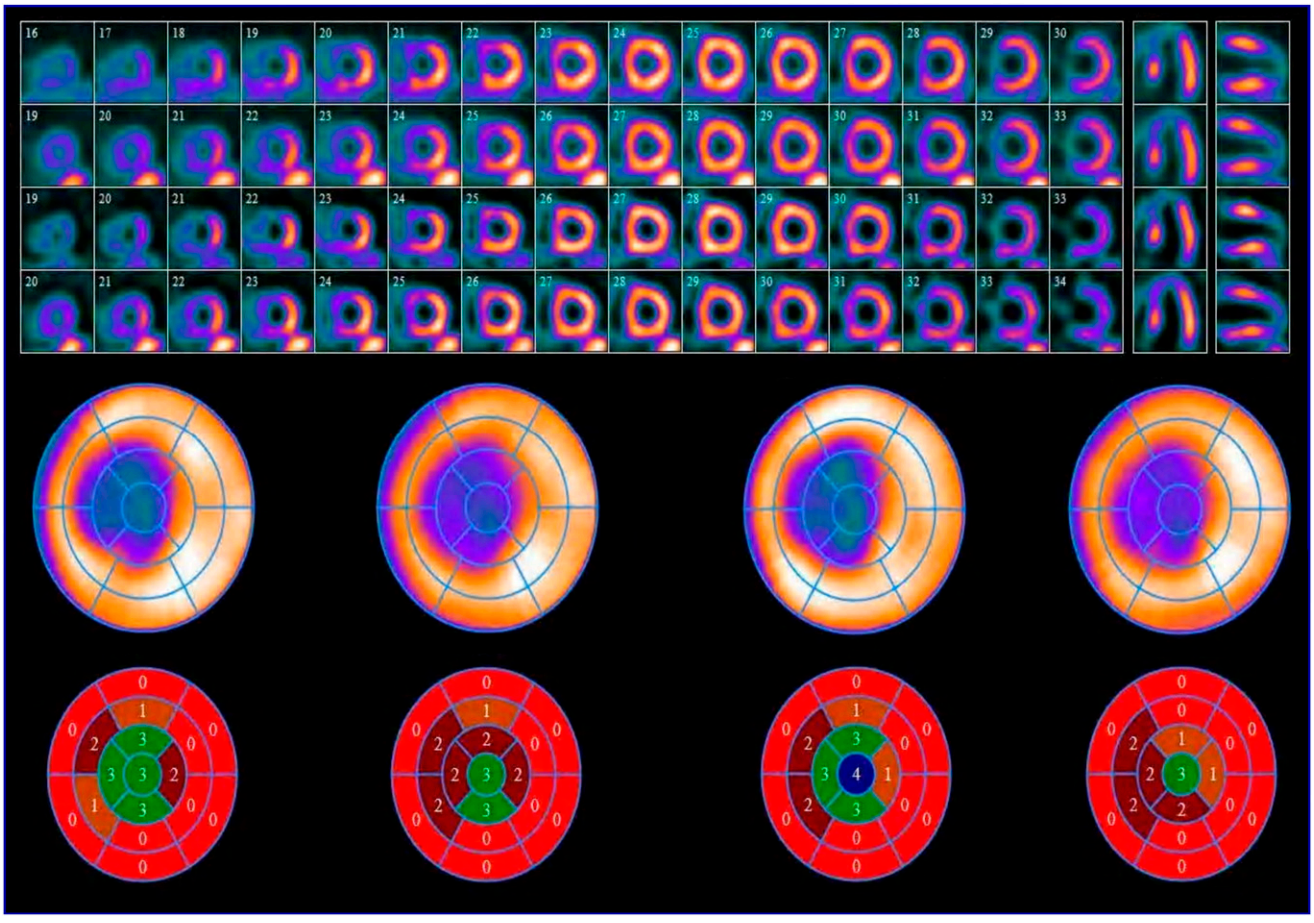

**FIGURE 3.** Corrected S/R low-energy high-resolution parallel-hole collimator (18 min) and IQ SPECT (4 min); 90% mid-left anterior descending artery.

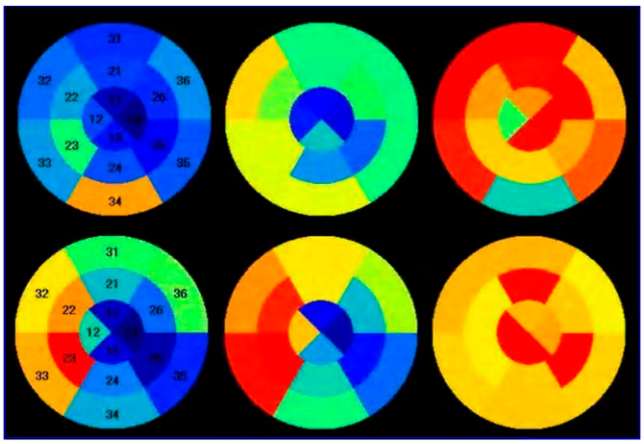

**FIGURE 4.** $^{82}$R-adenosine triphosphate stress/rest PET. Top: 2D rest, stress, and flow reserve. Bottom: 3D rest, stress, and flow reserve.

Another issue in multimodal imaging is coregistration, even when data are acquired in close temporal proximity. Misregistration is obviously a problem between CT angiography acquired during breathhold and PET or SPECT acquired over a longer time period. Nakazato et al. from Cedars-Sinai Heart Institute (Los Angeles, CA) and Unidad PET/CT Ciclotron (Mexico City, Mexico) reported on "Automatic alignment of myocardial perfusion PET with 64-slice coronary CT angiography on hybrid PET/CT" [1126]. They developed a program that helps coregister the data so that regional coronary and $^{82}$Rb perfusion can be aligned (Fig. 5).

Multimodality imaging involves not only PET/CT or PET/MR but also the correlation of MP with other cardiologic measurements, such as electrophysiologic characterization of the heart. Smith et al. from the University of Maryland School of Medicine (Baltimore, MD) reported on "Registration and fusion of cardiac electrophysiology voltage measurements with myocardial PET studies" [255]. They showed that the electrophysiologic study could be coregistered with the perfusion study or the viability study, in this case with $^{18}$F-FDG (Fig. 6), and correlated the various electrophysiologic characteristics with tracer distribution.

The new multimodality on the block is PET/MR. Our group at the Technische Universität Münich (Germany) have shown that using MR sequences one can do attenuation correction in much the same manner as with CT, without actually measuring the attenuation $\mu$ maps but by segmenting the body or the thorax in various ways and then applying standard $\mu$ values to it. Our first results indicate that the data are comparable to those obtained with PET/CT in the same patient population (Fig. 7).

Frank Bengel, MD, who delivered this year's Blumgart Lecture, presented a look at the future of clinical hybrid imaging protocols in which stress nuclear imaging for ischemia, LV function, and quantitative flow would be performed in 10 min with $<$2 mSv exposure to the patient; CT angiography for stenosis and plaque burden would be performed in 5 min with $<$2 mSv exposure; and CT with delayed enhancement for infarcts would be performed in 10 min with $<$2 mSv exposure. We must be fast, image with low radiation exposure to the patient, and provide a comprehensive exam, including perfusion, anatomy, and, in the future, tissue characterization, which can be accomplished either by CT or MR. It is important to emphasize the direction toward lower radiation exposure, which will be a major topic of discussion in future years.

## Diagnosis/Prognosis of Coronary Artery Disease (CAD)

A number of studies confirmed the high prognostic value of MP studies. One example was from Cerci et al. from the Universidade Federal do Paraná (Curitiba, Brazil), the University of São Paulo Medical School (Brazil), and Vanderbilt University Medical Center (Nashville, TN), who reported, "Ischemic myocardial perfusion SPECT is a strong predictor of death in women: a single center study in Brazil" [1106]. With a patient group of more than 2,000 women, they demonstrated again that MP imaging has an excellent prognostic capability to identify patients at higher risk. However, data also indicate the limitations of MP imaging. Ghadri et al. from University Hospital Zurich (Switzerland) reported that "Extensive coronary calcification unmasks obstructive CAD in patients with normal SPECT MPI" [1109]. This study indicated that a few patients with advanced CAD and massive coronary calcification may have normal perfusion scans. When evaluated with invasive

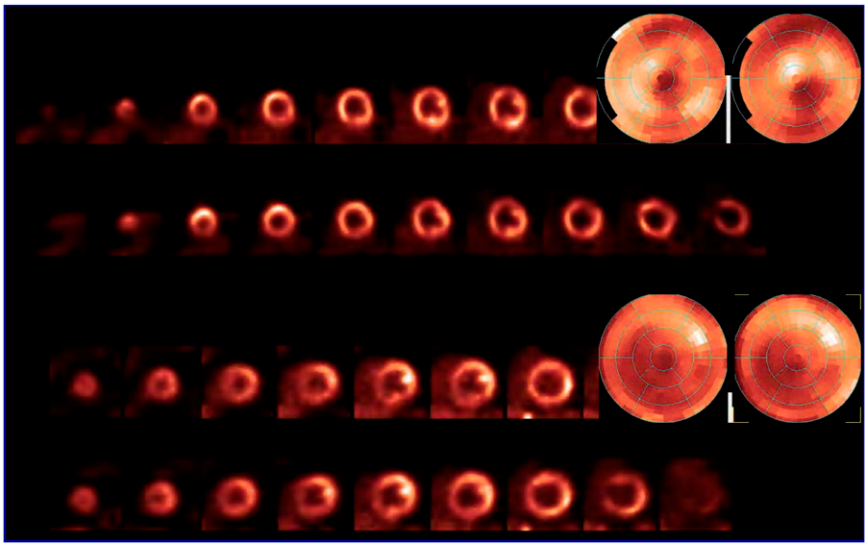

**FIGURE 5.** Attenuation-corrected cardiac MR/PET. Top row in each section: PET/CT; bottom row in each section: MR/PET. Larger images: left: PET/CT; right: MR/PET.

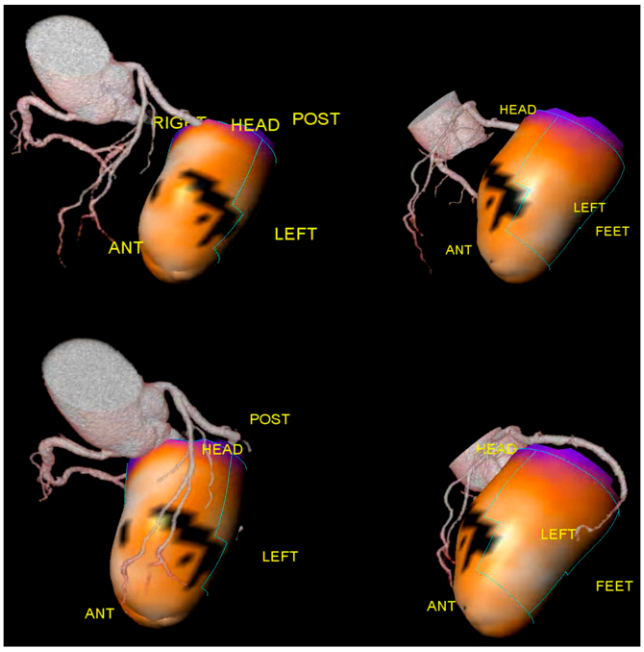


**FIGURE 6.** Automatic alignment of myocardial perfusion PET with 64-slice coronary CT angiography on hybrid PET/CT.

coronary visualization, it is clear that despite relatively normal perfusion these patients have higher incidences of 1-, 2-, and 3-vessel disease, supporting the notion of "balanced" ischemia as a cause for false-negative MP imaging in CAD.

The question is whether we might correct this underdiagnosis by adding absolute quantification of blood flow to our qualitative relative perfusion evaluation. This question was addressed by Danad et al. from the Free University Medical Center (Amsterdam, The Netherlands), who reported on the "Quantitative relationship between coronary artery calcium score and hyperemic MBF as assessed by hybrid $^{15}O$-$H_2O$ PET/CT imaging in patients evaluated for CAD" [3]. They showed the relationship between coronary calcification and CFR with patient-based and per-vessel–based analyses, indicating that patients with higher age have higher coronary calcification and decreased CFR.

This was addressed in a more detailed way in a larger patient cohort by Naya et al. from the Brigham and Women's Hospital (Boston, MA), who reported on the "Incremental prognostic value of quantitative CFR compared to coronary calcium score in patients with normal stress semiquantitative MP imaging" [58]. These researchers compared coronary calcification score and CFR in more than 900 patients. They pointed out that the only incremental value in the risk assessment is the impaired CFR, which turns out to be statistically superior to radiographic coronary calcification assessment.

The largest study to date looking at the prognostic power of $^{82}Rb$ imaging was also the winner of the Young Investigators' Award in clinical sciences. Murthy et al. from Brigham and Women's Hospital (Boston, MA) reported on "Incremental risk stratification with quantitative coronary vasodilator function assessment" [1]. They showed the relationship between outcome and CFR. The quantification of MBF at each level of relative stress perfusion defect showed an incremental value, with the highest, as expected, in patients with advanced disease. This study demonstrated clearly that quantitation of MBF has important prognostic implications. When the data were analyzed for high-, intermediate-, and low-risk patient groups, the impact was greatest in patients with intermediate risk as assessed by conventional stress testing and relative perfusion evaluation. When the quantitative CFR evaluation was added, about 50% of patients remained in the same category, but 30% had less risk associated and about 16% were considered as high risk. Outcomes in the 3 groups proved to be correctly characterized by the quantitative perfusion studies.

Danad et al. from the Free University Medical Center (Amsterdam, The Netherlands) reported on "Coronary risk factors and MBF in symptomatic patients evaluated for CAD, a quantitative $^{15}O$-$H_2O$ PET/CT study" [388]. They pointed out that it is difficult to define an absolute threshold for normal CFR, because gender, age, obesity, and hypercholesteremia influence the reference values. These pretest conditions must be taken into consideration when evaluating the threshold. They established a lower

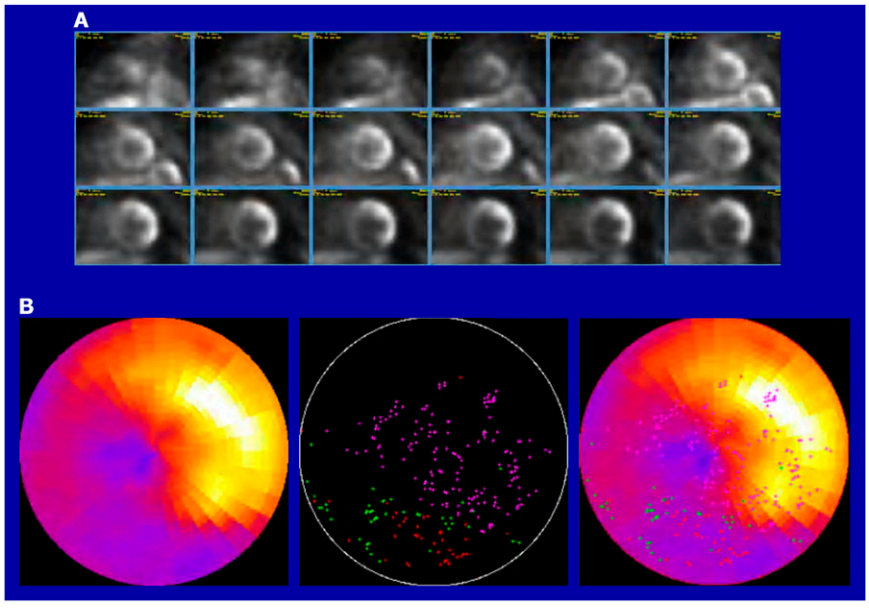


**FIGURE 7.** Registration and fusion of cardiac electrophysiology voltage measurements with myocardial PET studies. A. Short-axis FDG PET slices. B. Polar plots of: (left) $^{18}F$-FDG viability, (middle) discrete electrophysiologic (EP) voltage points (pink = normal [> 1.5 mV]; green = border zone [0.5–1.5 mV]; red = scar [<0.5 mV]), (right) fused PET/EP image.

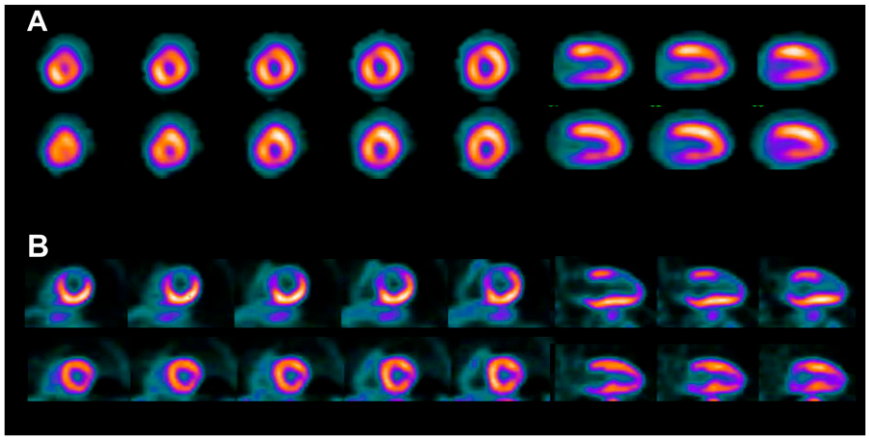


**FIGURE 8.** $^{18}$F-flurpiridaz phase 2 trial. 76-y-old man with significant left anterior descending defects on coronary angiography. Top rows: $^{99m}$Tc SPECT; bottom row: $^{18}$F-flurpiridaz PET. Overall image quality and resolution is superior with short-axis $^{18}$F flurpiridaz PET. Severe anterior and anteroseptal defects were noted on PET, but SPECT also shows a small, mild anteroseptal defect.

limit of hyperemic MBF in patients evaluated for CAD of ~1.5 mL/min$^{-1}$/g$^{-1}$ using $^{15}$O-$H_2O$ PET/CT. This is, of course, dependent on the technology used. They emphasized that it is important to provide quality control approaches to derive the best possible diagnostic value.

Many of us are anticipating the introduction of a fluorolabeled flow marker. Maddahi et al. from the University of California at Los Angeles (UCLA) School of Medicine, Cedars-Sinai Medical Center (Los Angeles, CA), Lantheus Medical Imaging, Inc. (Billerica, MA), and Tufts Medical Center (Boston, MA) reported on "Phase 2 clinical comparison of flurpiridaz $^{18}$F injection PET and SPECT MP imaging for diagnosis of CAD" [59]. Figure 8 is an example of a patient who underwent $^{99m}$Tc SPECT and $^{18}$F-flurpiridaz PET at different locations. I believe this is an extreme example, showing only a mild abnormality on SPECT and a distinct perfusion abnormality on PET. Although this example emphasizes the difficulty in comparing studies performed at different time points, the improved image quality is very promising. We must wait for results of a phase 3 evaluation to compare the diagnostic accuracy of both tests.

Some of the same patients were part of the study by Huang et al. from the UCLA School of Medicine and Lantheus Medical Imaging, Inc. (Billerica, MA), who reported on "Streamlined quantification of absolute MBF at rest and stress with flurpiridaz $^{18}$F injection PET in normal subjects and patients with CAD" [1114]. They showed an increase in MBF during stress in areas not affected by CAD; in the areas affected it was clearly decreased. It is this difference that makes this test attractive for characterization of CAD.

New tracers are on the horizon. Mou et al. from Beijing Normal University, the Chinese Academy of Medical Sciences, and Capital Medical University (all in Beijing, China) reported on "Preparation and in vivo evaluation of $^{18}$F-FP1OP for MP imaging with PET" [77]. This tracer targets the MC1 or the mitochondrial respiratory chain and has a high uptake in the myocardium (Fig. 9). In contrast to flurpiridaz, it has a rapid washout from myocardium, which may offer some advantages if developed into a product, both in terms of radiation exposure and rest/stress studies.

$^{18}$F-FDG has been widely used to characterize inflammatory plaques. Ogawa et al. from the Hamamatsu University School of Medicine (Japan) reported on the "Effect of macrophage foam cell formation on $^{18}$F-FDG uptake in atherosclerotic plaques" [57]. This study very nicely addressed the biology behind the uptake of FDG in atherosclerotic plaques, indicating that there is activation in the plaque, converting macrophages to foam cells, with upregulation during the first 24 h, especially notable in hexokinase, which is responsible for the increased FDG uptake.

A study from Hoffman et al. from the University of Utah (Salt Lake City) looked at "Uptake of 2-deoxyglucose analogs by thrombotically activated cells" [327]. They showed that thrombocytes also increase FDG uptake in the context of acute inflammation, emphasizing the dynamic nature of biology monitored with FDG uptake.

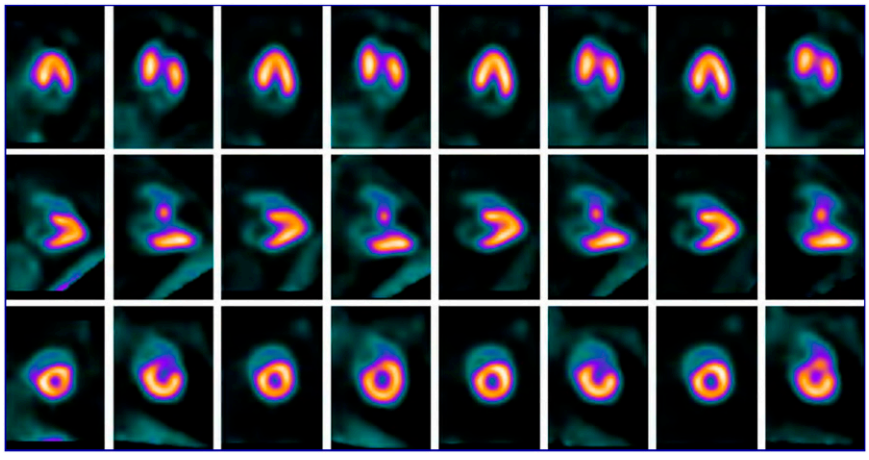

**FIGURE 9.** Cardiac PET images of Chinese miniswine: alternating healthy and acute myocardial ischemia images with 37 MBq $^{18}$F-FP1OP. Uptake of perfusion deficit areas was much lower than that of normal tissue in acute ischemia model.

**FIGURE 10.** Psoriasis is associated with increased aortic inflammation as measured on FDG PET/CT—a novel observation.

Another area of inflammation monitoring was described by Saboury et al. from the University of Pennsylvania School of Medicine (Philadelphia), who reported that "Psoriasis is associated with increased aortic inflammation as measured on FDG PET/CT: a novel observation" [114]. Their data indicated that in patients with psoriasis increased vascular activity and increased FDG are seen in cutaneous lesions (Fig. 10), indicating that FDG is sensitive to inflammation in the vascular tree. These studies also showed that after treatment FDG uptake decreased.

Can we use FDG to identify vulnerable plaque? Cheng et al. from Cedars-Sinai Medical Center (Los Angeles, CA) and the Cleveland Clinic Foundation (OH) reported on "Coronary artery uptake of $^{18}$F-FDG at culprit sites of acute myocardial infarction and stable ischemic CAD after percutaneous coronary stenting" [1155]. In some patients FDG uptake was clearly seen in areas of intervention, indicating acute inflammation (Fig. 11). However, FDG imaging is challenging in the heart, where some patients have increased uptake of FDG in the myocardium and dietary interventions are needed to decrease myocardial FDG uptake. However, when data were summarized from 20 patients after acute myocardial infarction and 7 patients with stable CAD who underwent intervention, about a 45% incidence of increased FDG uptake was seen in the culprit lesion.

Our group addressed the same question and found a somewhat lower incidence of 20% focal FDG coronary uptake, as reported by Weissmueller et al. from the Technische Universität Münich (Germany) in "Molecular imaging of vascular $^{18}$F-FDG uptake with PET/CT in patients early after an acute coronary syndrome" [1121]. What is interesting is that in this population, patients who had increased uptake in the lesion responsible for the infarct also had uptake in a so-called "remote" reference vessels, indicating that inflammation resulting in a vulnerable plaque is not a localized phenomenon but involves the entire cardiovascular tree.

## Translational Research

Higuchi et al. from Johns Hopkins University and the Medizinische Hochschule Hannover (Germany) reported on "Electrophysiologic implications of PET-defined, active cardiac sarcoidosis" [1136] and won the award for best cardiovascular poster. They showed that focally increased FDG uptake was strongly correlated with implanted cardioverter defibrillator discharge, which is a complication in patients with myocardial sarcoidosis (Fig. 12). FDG accuracy was quite high, indicating that FDG may be useful not only for diagnosis of myocardial involvement but also for risk assessment of fatal arrhythmias. This hypothesis remains to be proven in prospective trials.

Herrerro et al. from the Washington University School of Medicine (St. Louis, MO) reported on "Cardiac iNOS PET imaging using $^{18}$F-NOS: a feasibility study in transplant patients under-

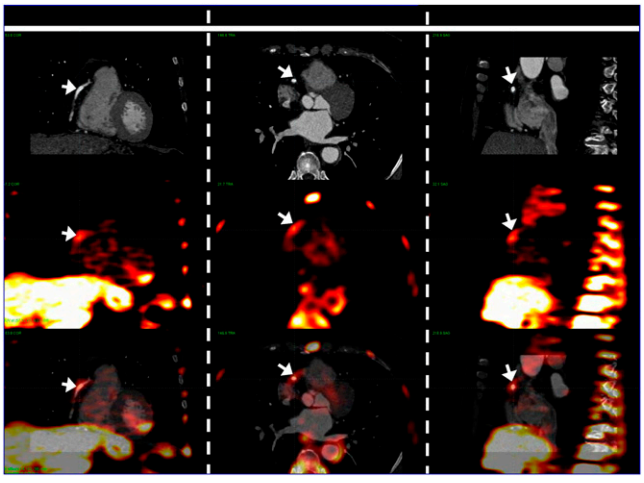

**FIGURE 11.** Visually apparent FDG uptake at the culprit site in a patient after percutaneous coronary stenting to proximal right coronary artery for acute myocardial infarction. Columns, left to right: Coronal, axial, and sagittal views. Rows, top to bottom: CCT only (arrows = stent), FDG PET only (arrows = uptake), coregistered CCT and FDG PET (arrows = stent).

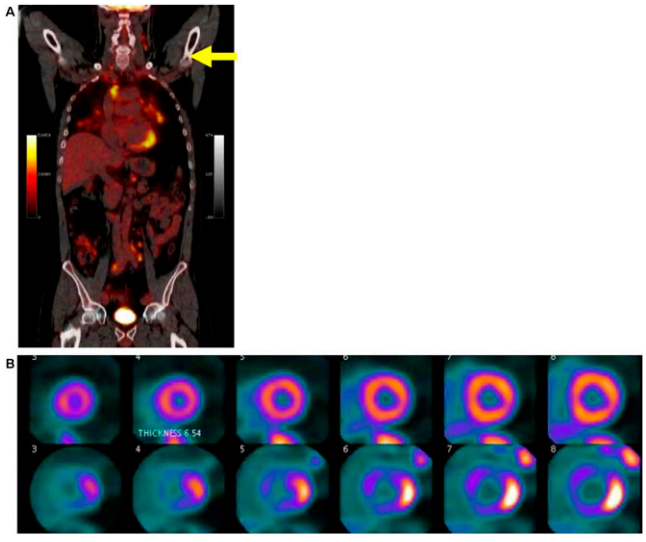


**FIGURE 12.** Electrophysiologic implications of PET-defined, active cardiac sarcoidosis. (A) Whole-body FDG PET. (B) Top: $^{82}$Rb PET; bottom: $^{18}$F-FDG PET. Focal myocardial uptake was associated more strongly with implantable cardioverter defibrillator discharge (accuracy 78%) than other clinical and imaging parameters. FDG PET may thus be useful not only in primary detection but also in risk stratification of patients with known cardiac sarcoidosis.

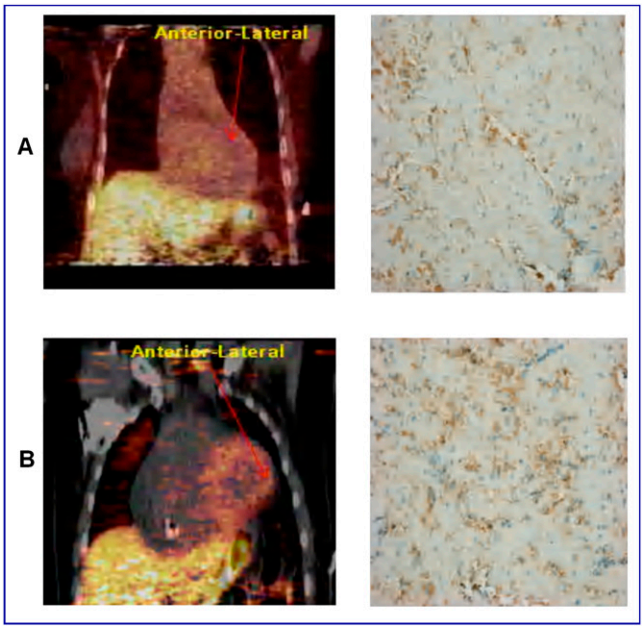


**FIGURE 13.** Cardiac iNOS PET/CT imaging using $^{18}$F-NOS.

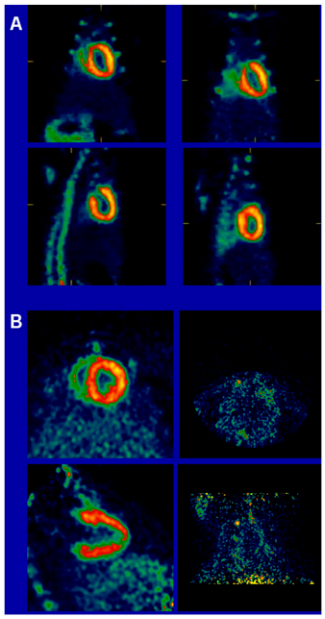


**FIGURE 15.** Imaging of sympathetic neuron impairment with 6-OHDA. Tissue biodistribution studies were performed in rats and rabbits with and without blockade of neuronal uptake-1 using desipramine at 60 min after LMI1195 injection. Top block: rats; bottom block: rabbits. Left panels: controls; right panels: with blockade of neuronal uptake.

going surveillance for allograft rejection" [331]. Their data indicated the potential of molecular imaging to identify acute inflammation in transplant rejection. iNOS is involved in pathways of inflammation. The group labeled an $^{18}$F-NOS to identify inflammatory activity in the heart. Figure 13 shows a patient with rejection and increased uptake compared with normal heart. However, these are very rapid kinetics, so the differentiation is only visible in the first 10 min. This appears to be promising but the value in management of patients with coronary transplantation remains to be evaluated clinically.

Bravo et al. from the Johns Hopkins University (Baltimore, MD) and the Medizinische Hochschule Hannover (Germany) reported on "Translational imaging of the myocardial angiotensin II type 1 receptor using $^{11}$C-KR31173 PET: from animal model to human application" [5]. This group won the cardiovascular young investigator award for basic science. Their newly introduced tracer showed good delineation of these receptors in the pig heart and somewhat less quality in the human heart, with much more heterogeneity (Fig. 14). This indicated the species differences in models as well the potential for visualizing angiotensin receptors, which are involved in the remodeling process in patients with heart failure.

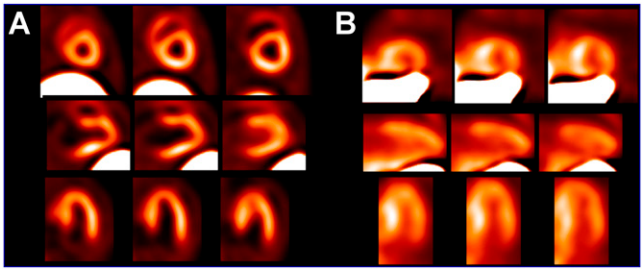


**FIGURE 14.** Imaging of the myocardial angiotensin II type 1 receptor using $^{11}$C-KR31173 PET. Left: representative pig heart. Right: representative human heart. Top rows: short axis; middle rows: vertical long axis; bottom rows: horizontal long axis.

The same species differences can be seen in the study by Bozek et al. from Lantheus Medical Imaging, Inc. (Billerica, MA), who reported on "Roles of cardiac norepinephrine uptake 1 and 2 in evaluation of LMI1195, a new cardiac PET neuronal imaging agent, in rats, rabbits, and nonhuman primates" [1099]. They showed that in the rat heart, the blockage of uptake 1, which is responsible for retention of tracer in the nerve terminal, had little effect on tracer kinetics, because the rat myocardium expresses uptake 2, which takes up the tracer independently of the presence of nerve terminals (Fig. 15). In the rabbit, blockage of uptake 1 significantly decreased retention, indicating the specificity of this tracer. We know from MIBG data that the rabbit is closer to the human than the rat as a model.

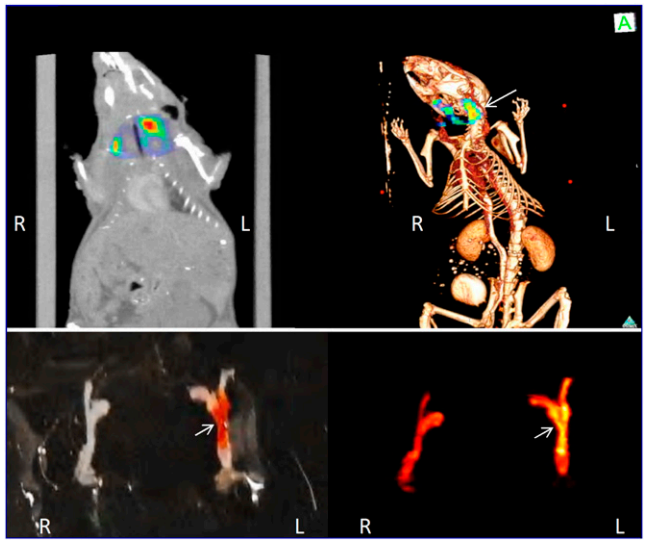


**FIGURE 16.** Fibrin-targeted near-infrared imaging of deep vein thrombosis in rat. Top rows: fluorescence molecular tomography/CT, jugular vein. Bottom: jugular veins ex vivo. Left column: (2D fusion, coronal); right column 3D fusion.

A look into the multimodalilty future was presented by Hara et al. from Massachusetts General Hospital (Boston, MA), who reported on "Molecular imaging of deep vein thrombosis using a new fibrin-targeted near-infrared fluorescence imaging strategy" [4]. Excellent regional uptake was coregistered with the CT using this optical imaging approach (Fig. 16). The ex vivo data clearly indicated localization of the signal with the thrombus. How much this can be translated to humans, however, is in question.

### Conclusion

In his Blumgart Lecture, Bengel discussed the long-term survival strategy for nuclear cardiology, which I like to cite as motivation for future researchers in our field. First, we must adapt to dynamic changes in the medical landscape, especially to link molecular imaging to therapy. The increasing specificity of therapeutic measures requires increasing specificity of diagnostic tools. Molecular imaging also provides the opportunity to create imaging-driven therapeutic strategies. We need to integrate increasing knowledge in medicine and try to identify patients who may benefit from specific targeted therapies. We must also look beyond organ borders; cell trafficking, immune signaling, inflammation, and angiogenesis occur in many disease representations and will be keys to prevention and regeneration. We finally must generate an integrative environment that maximizes imaging potential by training people in these various areas.

*Marcus Schwaiger, MD*
*Technische Universität München*
*Munich, Germany*

## Neurosciences

The dominant topic in neuroscience this year, as last year, was β-amyloid imaging, with the number of presentations increasing to 48 from 26 in 2010. The second major area was brain tumor imaging, with 33 presentations, up from 15 last year. Dopamine transporter (DAT)/vesicular monoamine transporter (VMAT) imaging was also very topical, with the release of a clinical DAT scanning agent in the United States. Small animal imaging, especially with microPET, continues to grow, with 28 presentations this year. Nonhuman primate imaging was the topic of 18 presentations at this meeting. We have an ever-increasing variety of radioligands used in neuroscience research—57 different ligands for various neuroreceptors, transporters, pathological markers, etc., were presented at this meeting. FDG PET, however, continues to play a major role and was the topic of 69 neuroscience presentations. The major areas of research are cognitive decline/dementia, the development and application of neuroreceptor imaging ligands, brain tumor investigation, and movement disorders. Good work is also being done in psychiatric disorders, drug and alcohol abuse, epilepsy, neuroinflammation, traumatic brain injury, stroke, and the effects of chemotherapy on the brain.

### β-Amyloid Pet

Chet Mathis and William Klunk at the University of Pittsburgh developed $^{11}$C-PiB, the first specific amyloid PET tracer and, in collaboration with Uppsala University, Sweden, performed the first human study in 2002. We now have literally thousands of studies being carried out each year with β-amyloid imaging ligands. A presentation from the Austin Hospital (Melbourne, Australia) and a consortium of researchers from 5 other Australian centers reported on "The consequences of Aβ deposition in aging and Alzheimer's disease [AD]: results from 366 elderly patients" [121]. The participants all underwent $^{11}$C-PiB PET imaging with longitudinal follow-up. The main findings included that age and genetics, as expected, have a major role in the presence of amyloid in the brain. A normal person in his or her 60s has an 11% risk of having a positive amyloid scan. This jumps to 32% in the 70s and to >50% in those older than 80 y. Within these decades the strong effect of genetics is apparent, with those individuals with the ApoE-ε4 gene allele, the most prominent gene associated with AD risk, being 3 times more likely to have a positive PiB scan than those without the gene. Serial studies in this cohort are being carried out and confirm that amyloid accumulation is a slow and gradual process, with PiB binding rising ~2%–4%/y in those with positive scans and on average by 1%/y in individuals with negative scans. Figure 17 shows a comparison of average rate of gray matter atrophy over 1 y in healthy elderly individuals with and without positive PiB scans. A greater rate of atrophy in brain areas typically most affected in AD is seen in those who have positive PiB scans. Looking at outcomes over 3 y in this study, "normal" older individuals who are PiB-positive also had about a 25% chance of converting to mild cognitive impairment (MCI) or AD, compared with a risk of only 3% in those with negative scans. Those who already had symptoms of

Christopher Rowe, MD

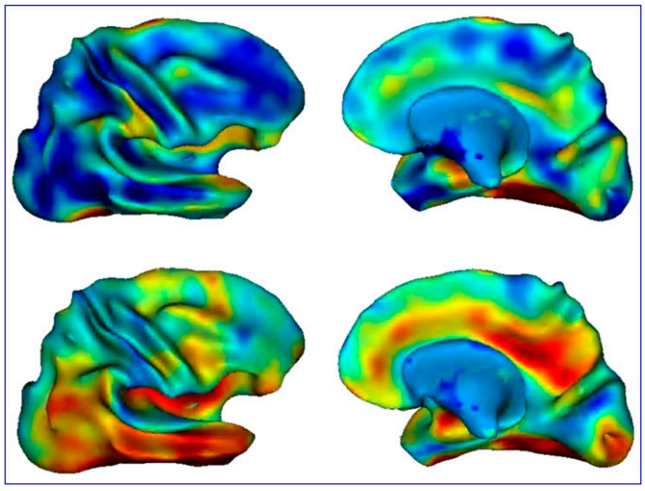

**FIGURE 17.** Average rate of atrophy over 1 y in healthy controls who were PiB-negative vs PiB-positive. Red areas indicate atrophic process beginning in individuals who are asymptomatic but have positive PiB scans.